DOI: 10.1002/anie.200803181

Catalyst Characteristics

Molecular Factors of Catalytic Selectivity

Gabor A. Somorjai and Jeong Y. Park*

Keywords:
adsorption · heterogeneous catalysis · nanoparticles · reaction intermediates · selectivity

Dedicated to the Catalysis Society of Japan on the occasion of the 50th anniversary

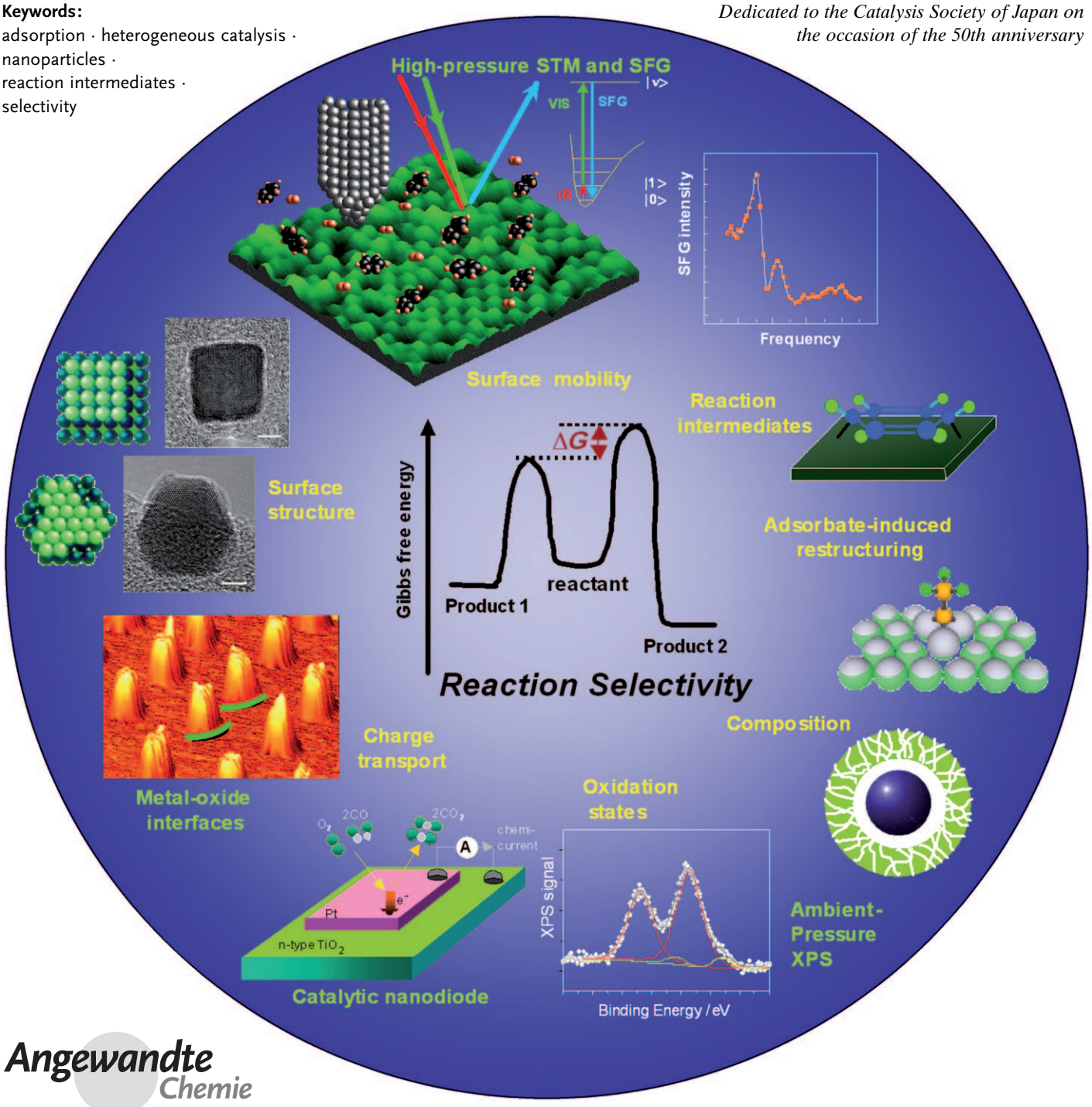

Selectivity—the production of one molecule out of many other thermodynamically feasible product molecules—is the key concept in developing clean processes that do not produce by-products (green chemistry). Small differences in the potential-energy barriers of single reaction steps control which reaction channel is more likely to yield the desired product molecule (selectivity), while the overall activation energy of the reaction controls the turnover rates (activity). Recent studies have demonstrated that tailoring parameters at the atomic or molecular level—such as the surface structures of active sites—gives turnover rates and reaction selectivities that depend on the nanoparticle size and shape. Here, we highlight seven molecular components that influence the selectivity of heterogeneous catalyst reactions on single-crystal model surfaces and colloid nanoparticles: surface structure, adsorbate-induced restructuring, adsorbate mobility, reaction intermediates, surface composition, charge transport, and oxidation states. We show the importance of the single factors by means of examples and describe in situ analyses that permit their roles in surface reactions to be investigated.

From the Contents

1. Introduction

During the 20th century, heterogeneous catalysis evolved into an important research area. Model surfaces were adopted and instrumentation was developed for molecular studies of surface chemistry (including the structures, dynamics, and chemical bonding of atoms and molecules at surfaces) while simultaneously measuring reaction rates and product selectivities.[1–3] Most of the studies were carried out by using catalytic reactions that afforded a single product, such as ammonia synthesis, carbon monoxide oxidation, or ethylene hydrogenation. The development of new and useful heterogeneous catalysts for carrying out multipath reactions with high selectivity and which lead to major gains in energy efficiency, as undesirable by-products are eliminated, are the goal of the 21st century.[4] Decades of research and development have produced industrial catalysts that possess nanosize features which contribute in a fundamental way to their function (activity and selectivity).[3] For porous materials (for example, those based on zeolites),[5–7] the pore size can exclude molecules with diameters larger than the pore from approaching the active site inside the pore, while smaller molecules can enter and react. For metal catalyst particles, the presence of sites with threefold symmetry can facilitate organic rearrangements that produce aromatic molecules. Atomic steps, kinks, and sites of special coordination properties can selectively break H–H, C–H, C–C, C=O, and O=O bonds. Oxide–metal interfaces are implicated in changing both the activity and selectivity of multipath reactions, such as the hydrogenation of carbon monoxide.[8] Recent advances in synthetic nanotechnology and in situ techniques have revealed correlations between catalyst selectivity and the size and shape of the metal catalyst particles as well as their location and bonding on the oxide support.[9–12]

In this Review, we highlight recent findings concerning the molecular factors that govern the reaction selectivities of transition metals, mainly platinum and rhodium, at temperatures below 600 K. In Section 2 we describe the challenge of fine-tuning the heights of the potential-energy barriers so as to control selectivity in heterogeneous catalysis. In Section 3, we emphasize that enzymes as well as heterogeneous and homogeneous catalysts can be regarded as nanoparticles. This observation drives the evolution of model catalyst surfaces from studies of single crystals to studies of nanoparticles with sizes of 1–10 nm. In Section 4, we describe the synthesis of nanoparticles through colloid chemistry, which appears at present to be the most versatile method for controlling the size and shape of nanoparticles. We show recent results on dendrimer-encapsulated platinum and rhodium nanoparticles that have cluster sizes of one nanometer or less. Section 5 is concerned with the fabrication and characterization of two- and three-dimensional nanoparticle systems. Then, in Section 6, we give examples of the depend-

[*] Prof. G. A. Somorjai
Department of Chemistry, University of California
Berkeley, CA 94720 (USA)
E-mail: somorjai@berkeley.edu
Prof. G. A. Somorjai, Dr. J. Y. Park
Materials Sciences Division and Chemical Sciences Division
Lawrence Berkeley National Laboratory
Berkeley, CA 94720 (USA)

ence of the selectivity of the catalytic reaction on the particle size and shape; these properties appear to be major factors for developing catalysts with complete selectivity. We explore why, on a molecular scale, the nanocatalysts are dependent on the particle size and shape. In Section 7, we discuss the influence of capping layers on the colloid nanoparticles on the catalytic activity and selectivity, and how these layers might be removed or modified. In Section 8, we list seven molecular factors that are responsible for the selectivity of catalytic reactions: surface structure (Section 8.1), adsorbate-induced restructuring (Section 8.2), adsorbate mobility (Section 8.3), reaction intermediates (Section 8.4), surface composition (Section 8.5), charge transport (Section 8.6), and oxidation states (Section 8.7). One example is given for each factor from surface science studies performed at Berkeley. The techniques that provide molecular information on catalytic surface reactions are introduced with a special emphasis on three instruments based on scanning tunneling microscopy (STM) that operates at high pressures,[13] high-pressure sum frequency generation (SFG) vibrational spectroscopy,[14] and ambient-pressure X-ray photoelectron spectroscopy.[15] The corresponding apparatus were developed recently in Berkeley. Finally, in Section 9, we argue for the importance of combined studies of enzyme, homogeneous, and heterogeneous catalyzed reactions under the same experimental conditions.

In this Review, we emphasize the need to focus on reaction selectivity, instead of activity, as the next great challenge of catalysis. Secondly, we show that nanoparticles can be used as model systems. Thirdly, we show the advance made in characterization techniques, which has permitted investigation of the catalyst surface at a molecular level under reaction conditions. We hope this Review illustrates the way to transfer results from model systems to industrial catalysis science. The integration of catalysis research with synthesis, characterization, and reaction kinetic studies has accelerated progress in the field.

2. Selectivity in Heterogeneous Catalysis

Product selectivity is essential in developing processes that yield the desired molecules in multipath reactions with complete selectivity. Instead of a single potential-energy barrier that is reflected by the activation energy for the formation of a product, there are several potential-energy barriers with small energy differences.[16–19] We chose organic reactions that are catalyzed by platinum and rhodium at temperatures below 600 K and usually form two different product molecules. The corresponding potential-energy plot for the competitive formation of two products is depicted in Figure 1.[1,17] This relative energy difference between the activation energy barriers determines the reaction selectivity. Figure 1 shows that very small changes, such as 2 kcal mol^{-1}, between potential-energy barriers completely change the product distribution. These changes can be induced by coadsorbates, small structural changes, or the addition of electron donors or acceptors, which change the binding energies of reaction intermediates or adsorbed reactants or products.

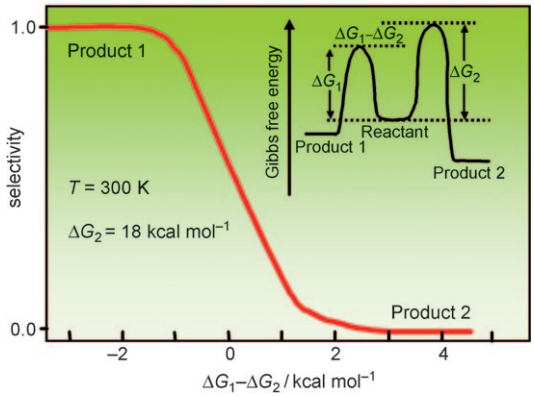

Figure 1. Potential-energy plot illustrating selectivity in heterogeneous catalysis. The relative heights of the activation barriers for different reactions determine the selectivity of catalytic processes.[17]

In general, the relative heights of the activation energy barriers are dependent on the atomic structure as well as on the electronic and chemical properties of the catalyst surfaces. Controlling the relative barrier height to change the reaction selectivity requires a good understanding of the roles played by the structural, dynamic, and electronic properties of the surfaces, which induce the desired chemical change.[20–23] We shall show that the shape and size of nanoparticles can be

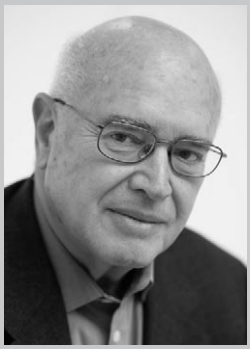

Gabor A. Somorjai was born in Budapest, Hungary, in 1935, and received his PhD from the University of California, Berkeley in 1960, where he is now Professor of Chemistry. He has received numerous awards, including the Priestley Medal (2008), the Langmuir Prize (2007), the National Medal of Science (2002), the Wolf Prize (1998), and the Peter Debye Award (1989). He has worked with more than 120 PhD students and 250 postdoctoral fellows. He has written three textbooks, and is the author of more than 1000 papers on surface chemistry, heterogeneous catalysis, and solid-state chemistry.

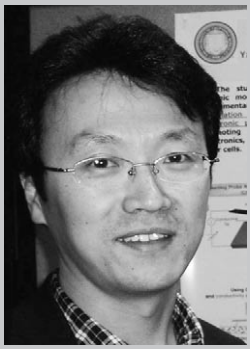

Jeong Young Park is a staff scientist at the Lawrence Berkeley National Laboratory. He received his PhD in Physics from Seoul National University in 1999. He spent two years at the University of Maryland working with Professor Ellen Williams and then joined the group of Professor Miquel Salmeron in 2002 where he carried out postdoctoral research. His research interests include the fundamental aspects of energy dissipation in friction and chemical reactions at surfaces and interfaces.

important factors that affect the reaction selectivity, because the surface structure is determined by their shape,[9,24] and the number of steps and kinks as well as the oxidation states (which change the electronic structures of the surface) are directly correlated with the size of the nanoparticles. Not only the catalysts but also the types of reactions (reactants and products) and reaction conditions (temperature, pressure, reaction time, and nature of the catalyst support) can affect the pathways during the multipath catalytic reactions because they alter the reaction intermediates and the surface mobilities. At the molecular level, seven key factors can be identified that influence the relative heights of the activation energy barriers, and thus enable the reaction selectivity to be tuned.

3. Catalysts are Nanoparticles—New Model Surfaces

Single crystals have been used for decades as model surfaces for studies of metal catalysis.[1,16,25] In fact all catalysts are nanoparticles, not just heterogeneous metal catalysts, but also enzymes and homogeneous catalysts (Figure 2). Cytochrome *c*, which is one of the over 3000 enzymes that function in the human body (Figure 2a), is 4 nm in size with its protein shell wrapped around it. The active site (heme) of the enzyme is 1.4 nm.[26] A typical homogeneous catalyst used for olefin polymerization with a single active site is the titanium complex shown in Figure 2b that is 1.6 nm in size.[27] The size of the platinum or rhodium nanoparticles in heterogeneous catalysts are 1–10 nm. Figure 2c shows a scanning electron microscopy (SEM) image of 8 nm sized $Pt_{0.5}Rh_{0.5}$ nanoparticles deposited on a silicon wafer by using the Langmuir–Blodgett technique.[28] It is important to understand how nanoparticles function in their roles as catalysts as they are used in nature and in the chemical technologies.

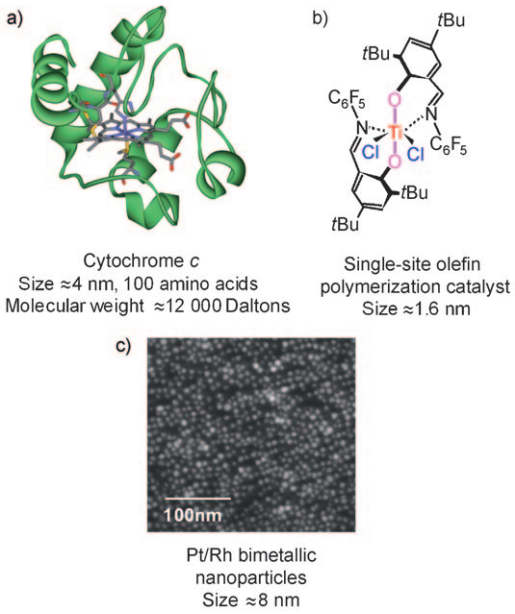

Figure 2. Most heterogeneous and homogeneous catalysts as well as enzymes are nanoparticles. a) The cytochrome *c* molecule. b) A titanium-based single-site homogeneous polymerization catalyst. c) SEM image of 8 nm monodispersed Pt/Rh bimetallic nanoparticles deposited on a silicon substrate.

Advances in nanoscience has made it possible to fabricate metal nanoparticles in the 1–10 nm regime, which is identical to the sizes of the heterogeneous metal catalysts used as industrial catalysts. As a result, model studies could be extended from single-crystal metal surfaces to nanoparticles of controlled shape and size and would also allow a "bridging of the materials gap" between crystal surfaces and nanomaterials that are used in industrial catalytic processes.[29,30] Single-crystalline metals used for modeling industrial catalysis inherently lack the complexity needed to uncover many of the factors important for catalytic turnover and selectivity. For example, considerations such as metal–support interactions and the size of the metallic cluster are of extreme importance to catalytic applications. To overcome this problem, several new model systems have been proposed and utilized (Figure 3).

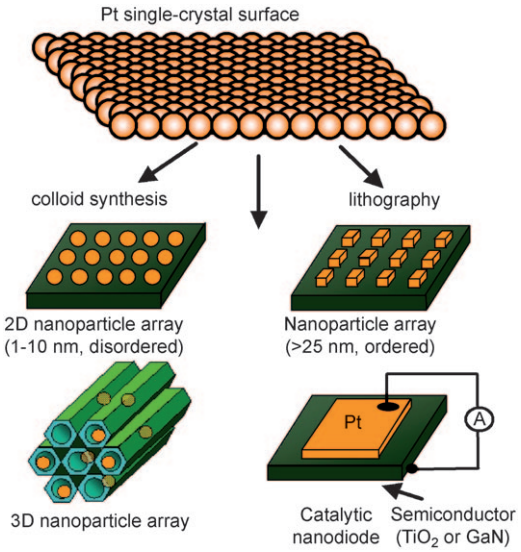

Figure 3. Evolution of model surface systems: from a single-crystal surface to nanoparticles, nanowires, and nanodiodes.

There is a great deal of experimental evidence indicating that the interface between the metal nanoparticle and the oxide support is an important catalytic site. Since heterogeneous metal catalysts are usually nanoparticles that are deposited on oxide supports, oxide–metal interfaces are major components of every catalyst system. Since the early studies by Schwab and Koller,[31,32] evidence has accumulated that the oxide–metal interfaces are responsible for the increase in activity and change of selectivity for many chemical processes. This phenomena has been exploited in the design of the "strong metal–support interaction (SMSI)" catalyst systems.[8,33]

For the production of SMSI catalysts, platinum nanoparticles and nanowires have been fabricated on oxide surfaces (such as oxidized silicon wafer) by using lithography

techniques. Platinum nanoparticles of 50 nm in size have been fabricated by electron beam lithography, which utilizes high-resolution pattern writing and an electron-sensitive resist/etching.[34–37] It was found that when the metal was poisoned by adsorbed CO, the turnover rate of ethylene hydrogenation was proportional to the oxide–metal periphery area, which suggests that the oxide–metal interface functions as a reactive site.[36] Another important property of oxide–metal interfaces is the generation of "hot" electrons during exothermic catalytic reactions. The resulting flow of charge occuring at the Schottky barrier formed at certain oxide–metal interfaces has chemical consequences,[38–41] as will be described in more detail in Section 8.6. We believe this charge flow is one of the important molecular factors which influences reaction selectivity in heterogeneous catalysis.

4. Nanoparticle Synthesis Controlled by Colloid Chemistry

Our focus has been on monodispersed platinum, rhodium, and bimetallic nanoparticles with well-controlled shape. By using hexachloroplatinic acid or rhodium acetyl acetonate as precursor monomers, it is possible to produce monodispersed metal nanoparticles, each coated with a polymer layer that prevents aggregation in solution (Figure 4).[11,42,43] Under

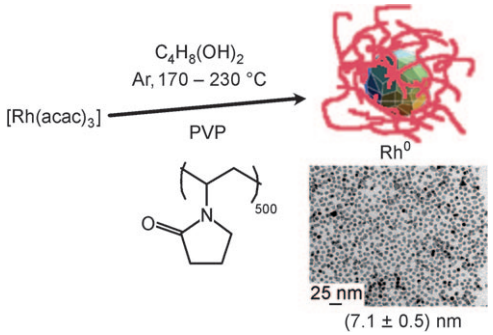

Figure 4. One-step synthesis of monodispersed rhodium nanoparticles. acac = acetylacetonoate.

well-defined conditions, the particle size is proportional to the monomer concentration and can be controlled by changing the monomer concentration. Under optimized reduction conditions, it was possible to control the size and shapes of the platinum or rhodium nanoparticles.[44–47] Figure 5 shows the corresponding platinum nanoparticles. High-resolution transmission electron microscopy (HRTEM) together with electron diffraction analysis reveals the shape of the nanoparticles.[44] These monodispersed nanoparticles with uniform size and shape can be deposited as a two-dimensional film by using the Langmuir–Blodgett technique. The nanoparticles can also be deposited in a mesoporous, three-dimensional oxide framework at much higher surface concentrations.[48] Studies of these different nanoparticle arrangements show that they give model surfaces that approximate the size and morphology of nanoparticles currently used in chemical technology.[49]

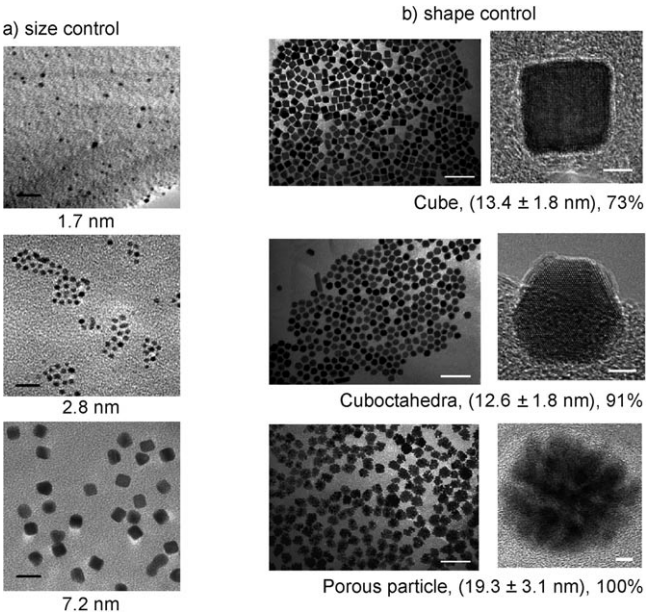

Figure 5. Monodispersed platinum nanoparticles of 1.7–7.2 nm size (a) and with well-controlled cubic or cuboctahedral shapes (b). Scale bar in (a): 10 nm, scale bar in (b): 50 nm (left) and 5 nm (right). The % values in (b) refer to the % of nanoparticles with the corresponding shape.

Recently, dendrimer-encapsulated metal nanoclusters have been explored for catalysis.[50–53] The structure and chemical properties of dendrimers—quasispherical hyperbranched polymers—can be controlled by changing the core structure, the number and type of the duplicating units, and the terminal functional groups (Figure 6). Poly(amidoamine)s (PAMAMs) are the most popular ones used in the synthesis of metal nanoparticles. Single metallic and bimetallic nano-

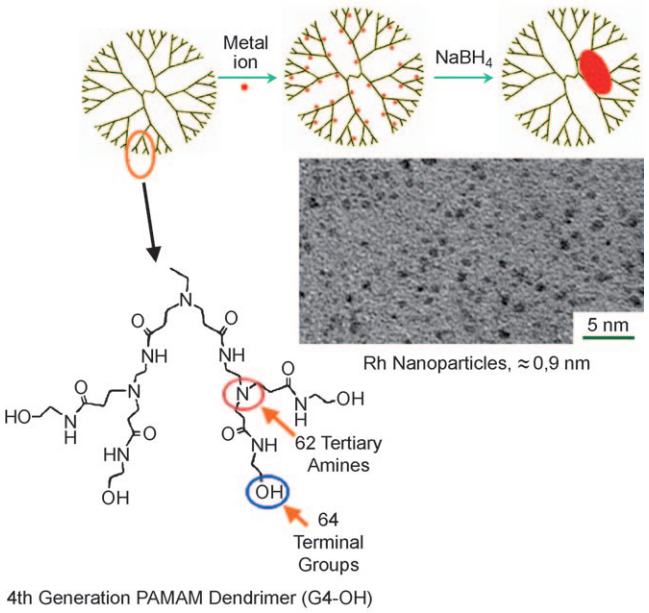

Figure 6. Synthesis of small monodispersed rhodium nanoparticles (≤1 nm) in dendrimers.

particles having dimensions less than 3 nm have been prepared within the cavities of high-generation (4th or higher) PAMAM dendrimers.[54] The size distribution of the metal nanoparticles synthesized within dendrimers is very narrow due to the well-defined composition and structure of the dendrimer template. Recently, we have successfully synthesized monodispersed platinum and rhodium nanoparticles ranging from 0.8 to 1.6 nm encapsulated within fourth generation PAMAM dendrimers.[55]

5. Characterization and Catalytic Reactions of Two- and Three-Dimensional Metal Nanoparticle Catalyst Systems

Once nanoparticles are synthesized, they can be placed on a Langmuir–Blodgett trough and fabricated into monolayer films at various densities.[49] The average interparticle spacing can be tuned by varying the surface pressure. This approach has the advantage of controlling the size and composition of the nanoparticles synthesized through this colloidal route before an oxide–metal interface is formed between the nanoparticles and the substrate. The particles are capped with an organic surfactant or a polymer, which prevents aggregation during synthesis in solution. A variety of organic coatings have been used, including tetradecyltrimethylammonium bromide (TTAB), hexadecylamine (HDA), hexadecylthiol (HDT), and PVP (poly(vinylpyrrolidone)). Figure 7a shows a TEM image of two-dimensional platinum nanoparticles coated with TTAB on a silicon oxide grid.

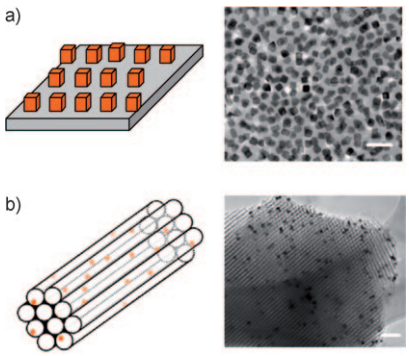

Figure 7. TEM image and schematic representation of a) a two-dimensional arrangement of TTAB-coated platinum nanoparticles and b) a three-dimensional arrangement of platinum nanoparticles encapsulated in mesoporous silica (SBA-15).

The nanoparticles can also be incorporated into mesoporous oxides with high surface areas (such as SBA-15)[7,56] or mesocellulous silica foams (MCF)-1)[57] by sonication or by synthesizing the mesoporous channels around the nanoparticles in the same solution. A TEM image of the platinum nanoparticles encapsulated in mesoporous silica with a channel structure (SBA-15) is shown in Figure 7b. The resulting 3D model nanoparticle catalyst system has a surface area of over 1 $m^2 g^{-1}$.

We have utilized many techniques for the characterization of the chemical, physical, and electronic properties of nanoparticles. Infrared and Fourier transform infrared spectroscopy, Raman spectroscopy, Auger spectroscopy, X-ray photoelectron spectroscopy, small-angle X-ray scattering and X-ray diffraction, physisorption, and chemisorption are techniques that enable the study of two- or three-dimensional nanoparticle arrangements (Table 1).

Table 1: Methods for studying two- or three-dimensional nanoparticles.

Ex situ characterization
transmission electron microscopy (TEM)
X-ray diffraction (XRD)
diffuse reflectance UV/Vis spectroscopy
X-ray photoelectron spectroscopy (XPS)
scanning electron microscopy (SEM)
chemisorption, physisorption
small-angle X-ray scattering (SAXS)
energy-dispersive X-ray analysis (EDX)
thermogravimetric analysis (TGA)
temperature programmed oxidation (TPO)
inductively coupled plasma with optical emission spectroscopy (ICP-OES)
In situ characterization
high-pressure scanning tunneling microscopy (HP-STM)
high-pressure sum frequency generation spectroscopy (HP-SFG)
ambient-pressure X-ray photoelectron spectroscopy (APXPS)
diffuse reflectance infrared spectroscopy (DRIFTS)
UV-Raman and surface enhanced raman spectroscopy (SERS)
transmission electron microscopy (TEM)
tapered element oscillating microbalance (TEOM)
thermogravimetric analysis (TGA)
UV/Vis diffuse reflectance spectroscopy
X-ray diffraction (XRD)
small-angle/wide-angle X-ray scattering (SAXS-WAXS)

Two types of reactors have been used to study catalytic turnover. The activity and selectivity of monolayers of nanoparticles were studied by a batch reactor, equipped with a recirculation pump, similar to that used for studies on single-crystal metal samples. A schematic representation of this catalytic reactor is shown in Figure 8a. Active metal nanoparticles are deposited by Langmuir–Blodgett techniques onto a planar support such as a silicon wafer. Typically, there are 10^{14} to 10^{15} active metal sites on the surface in a 2D system that are available for catalysis. The schematic representation of a three-dimensional system is shown in Figure 8b, where the reaction is performed in differential reactors. The active metal nanoparticles are supported on mesoporous oxides, where they are deposited by capillary inclusion or during hydrothermal growth of the oxide. In such systems there are typically 10^{16} to 10^{18} active metal reaction sites available for catalysis.

6. The Influence of the Nanoparticle Size and Shape on Reaction Selectivity

In this section, we provide several examples of how the size and shape of nanoparticles influence reaction selectiv-

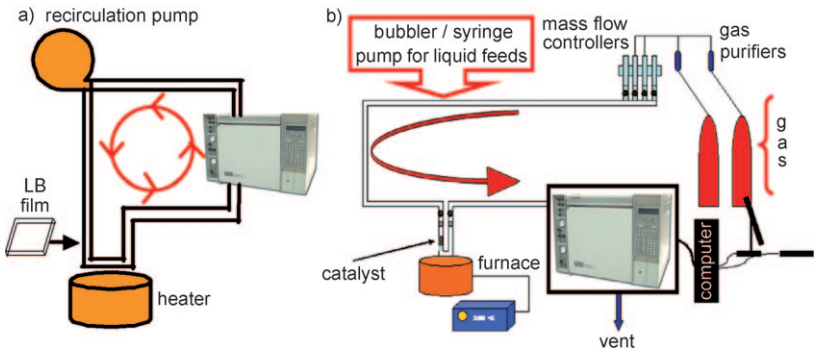

Figure 8. Schematic representation of a catalytic batch reactor for studies of two-dimensional catalysts with small areas (a), and a flow reactor for studies of three-dimensional catalyst systems with large surface areas (b).

ities. Typical multipath reactions utilized to study the reaction selectivity at the molecular level are shown in Scheme 1.

Figure 9 shows the dependence of the reaction selectivity on the particle size for the hydrogenation/dehydrogenation of cyclohexene and the hydrogenation of crotonaldehyde.[49] In the first example, the formation of benzene decreases as the size of the nanoparticles increases. The reason for this is that the activation energy for the dehydrogenation of cyclohexene to benzene increases with increasing particle size, while the activation energy for the hydrogenation to cyclohexane is constant and remains unchanged as the particle size increases.

We studied the effect of the nanoparticle size on the selectivity of the hydrogenation of benzene[58] to cyclohexane (C_6H_{12}) and cyclohexene (C_6H_{10}) on a Pt(111) surface; cyclohexene was the only product formed on the (100) surface. We found that platinum nanoparticle catalyst shaped as cuboctahedra, give rise to both C_6H_{12} and C_6H_{10}, just like the (111) surfaces of single crystals. When the catalyst surfaces are cubes, C_6H_{10} is formed as the only product, similar to the (100) surface of a single crystal (Figure 10).[24] This result indicates that the single crystals and the nanoparticles show the same surface-structure dependence and shape selectivity, thus indicating that the two types of surfaces behave similarly despite their difference in size.

The use of dendrimers as supports enables small nanoparticles to be produced.[55] The

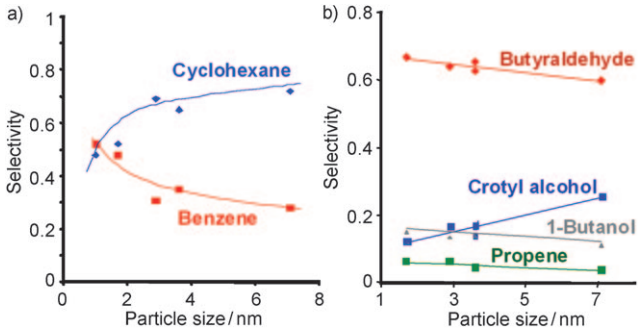

Figure 9. The dependence of the selectivity of cyclohexene hydrogenation/dehydrogenation (a) and crotonaldehyde hydrogenation (b) on the size of the platinum nanoparticles.

dendrimer cavities stop the growth of nanoparticles at around 1 nm and, in this way, the catalytic activity of small clusters of metals such as rhodium or platinum clusters with 20–30 atoms can be investigated (Figure 6). Figure 11 shows how the particle-size dependence in this small particle size range is much more dominant than the particle-size dependence with larger nanoparticles for the hydrogenation of pyrrole to pyrrolidine and *n*-butylamine.

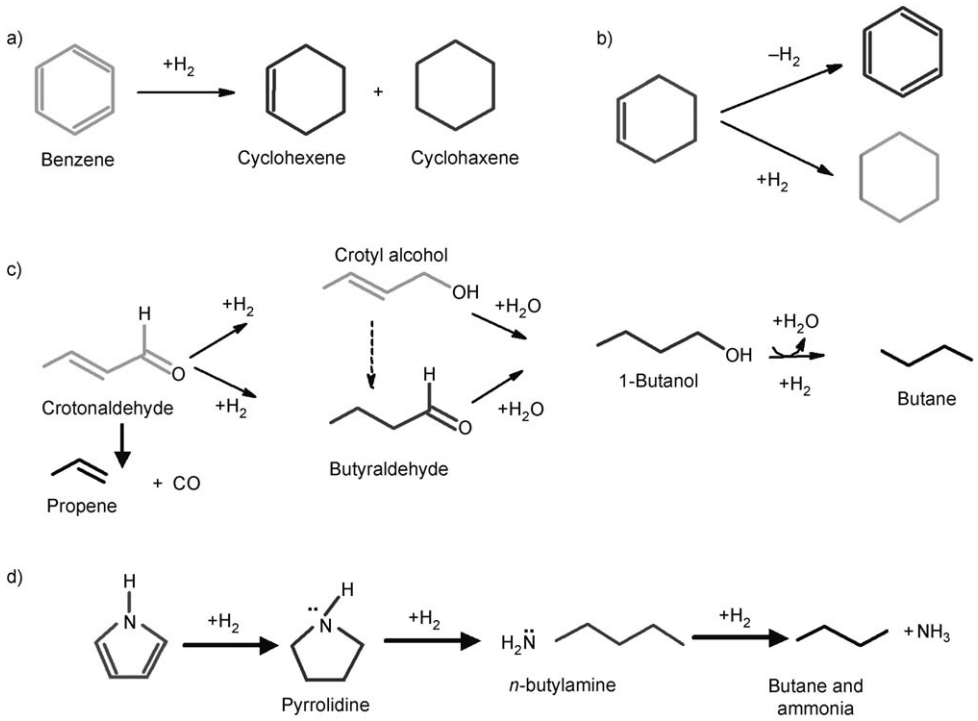

Scheme 1. The multipath reactions considered for understanding molecular selectivity: a) Hydrogenation of benzene, b) hydrogenation/dehydrogenation of cyclohexene, c) hydrogenation of crotonaldehyde, and d) hydrogenation of pyrrole.

7. The Role of Capping Layers on Nanoparticles in Catalytic Reactions

Several organic materials have been used to coat nanoparticles. These capping

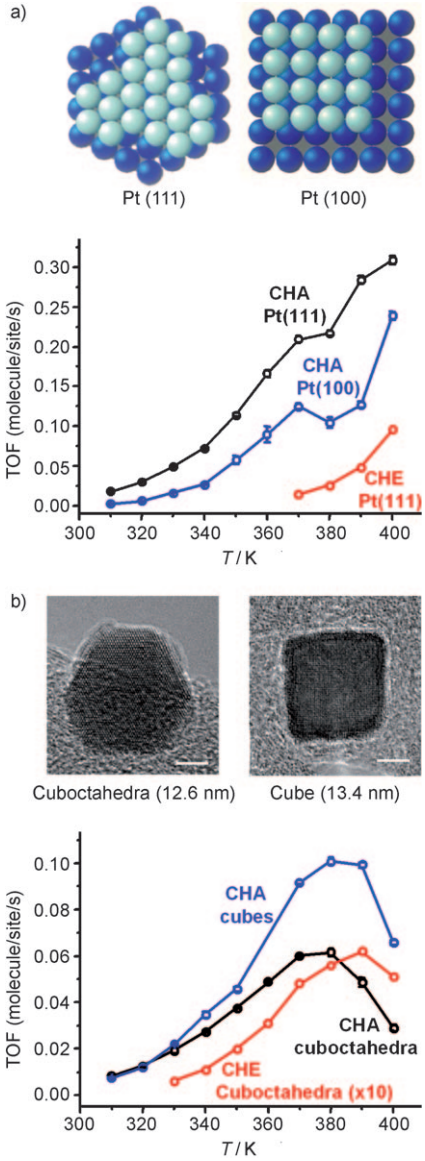

Figure 10. Turnover rates of cyclohexene and cyclohexane formation during the hydrogenation of benzene on Pt(111) and Pt(100) surfaces (a), as well as the cubic and cuboctahedra platinum nanoparticles (b), which demonstrate the similarities between the single-crystal and nanoparticle surfaces. CHA = cyclohexane, CHE = cyclohexene.

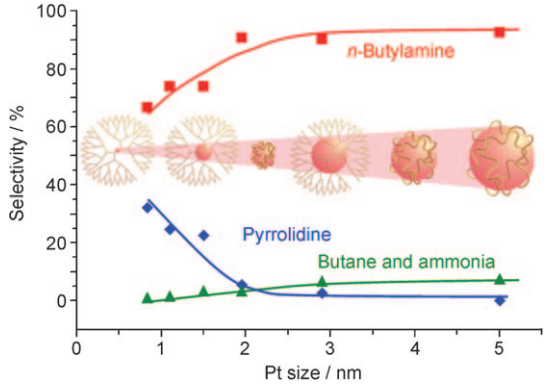

Figure 11. Dependence of the selectivity of the hydrogenation of pyrrole (4 Torr pyrrole, 400 Torr H_2, 413 K) on the size of the platinum nanoparticles encapsulated in a dendrimer or PVP.

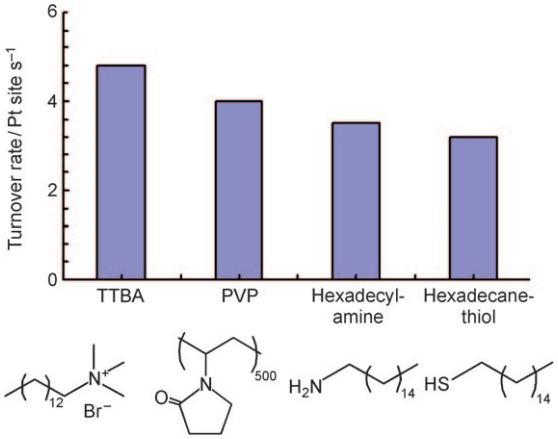

Figure 12. Turnover rates of nanoparticle arrays with different capping layers during the oxidation of CO (100 Torr of O_2, 40 Torr of CO, 513 K).

layers do not affect the catalytic reactions significantly because of their porous nature, which permits the reactant and product molecules to pass through them. We compared the catalytic activity of colloidal platinum nanoparticles coated with with four different organic layers—of TTAB, HAD, HDT, and PVP—in the oxidation of CO.[59] A 30% variation in the reaction turnover rates was observed (Figure 12).

The organic coatings can be removed after depositing the nanoparticles in either a two- or a three-dimensional mode by treatment with UV/ozone.[60] Figure 13 shows the preliminary results from the sum frequency generation vibrational spectroscopy measurements: the nanoparticles coated with the organic layers were first studied, and then with the organic layer removed, as evident by the disappearance of the CH–CH_2 stretches. The adsorption of benzene onto the surface of the platinum nanoparticles after treatment with UV/ozone is evident from the SFG vibrational spectrum.[61]

8. Seven Molecular Factors of Catalytic Selectivity

As shown earlier, reaction selectivity is determined by the relative energy difference between several activation energy barriers. From the viewpoints of reaction kinetics, selectivity requires control of the activation energies within a small fraction of their absolute value. However, the chemical and thermal stabilities of catalysts depend on the reaction conditions, such as temperature, pressure, reaction time, as well as the types of products and reactants. For catalytic reactions below 600 K, where the catalyst materials are comparably stable, we have so far identified seven molecular level factors that affect selectivity (Figure 14): 1) surface structure, 2) adsorbate-induced restructuring, 3) adsorbate mobility, 4) reaction intermediates, 5) surface composition, 6) charge transport during catalysis, and 7) oxidation state of the catalyst.

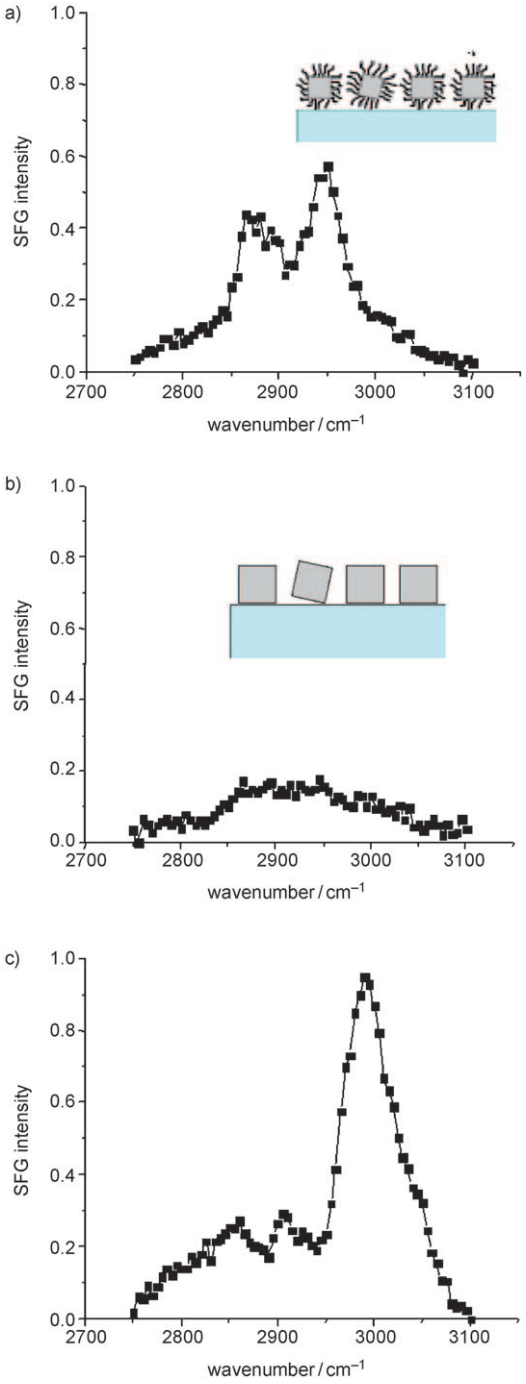

Figure 13. SFG spectrum of a) platinum nanoparticles (10 nm) coated with oleylamine ($CH_3(CH_2)_7CH{=}CH(CH_2)_8NH_2$), b) platinum nanoparticles after removal of the organic layer by exposure to UV/ozone for 200 min, and c) benzene adsorbed on the platinum nanoparticle surfaces after removal of the organic layer.

8.1. Surface Structure

For the study of surface structure, a system was developed that allowed both the reaction under high pressure and the surface—before and after reaction—to be analyzed under ultrahigh vacuum conditions (Figure 15a).[30]

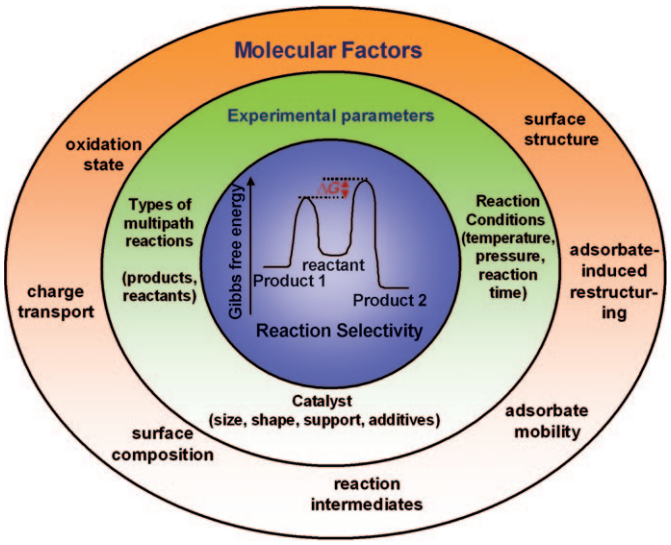

Figure 14. The seven molecular factors influencing the selectivity of a catalytic reaction.

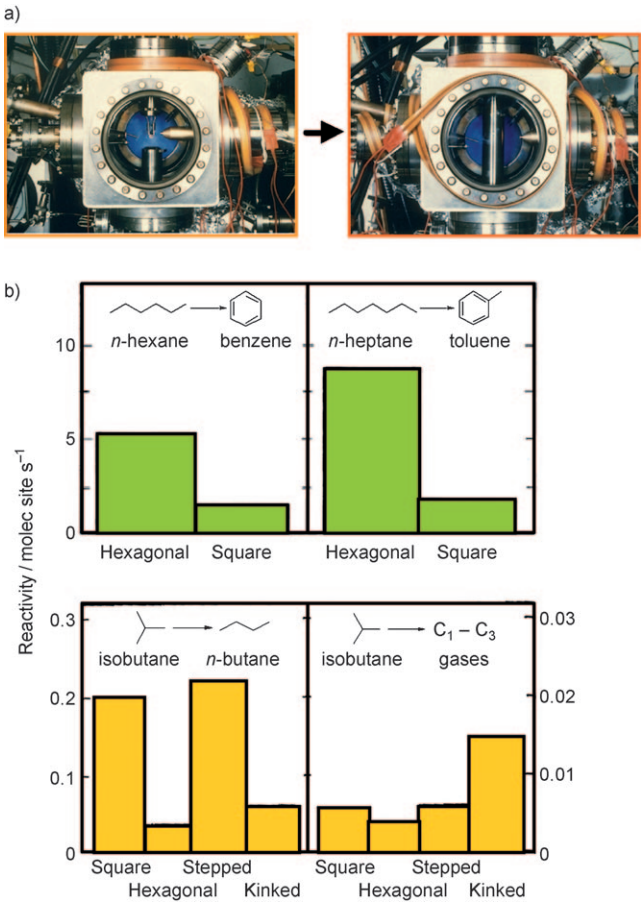

Figure 15. a) High pressure/ultrahigh vacuum system. The high-pressure cell is shown in both the open (left) and closed (right) positions. b) Structure dependence in the aromatization of alkanes (top) and rearrangement of small alkanes on the platinum surface.

The reforming reaction, where this multipath reaction scheme is important, produces high-octane gasoline of aromatic compounds and branched isomers from *n*-hexane

and *n*-heptane (with a near-zero octane number). Studies on the conversion of *n*-hexane on a platinum single-crystal surface indicate that the hexagonal (111) surface produces benzene as the major product, while the (100) faces prefer to catalyze isomerization reactions (Figure 15b).[62,63] The kink sites on the platinum surface break carbon–carbon bonds, which is an undesirable reaction; a catalyst poison is thus added to the reactant mixture in the form of H_2S that strongly adsorbes to the kink sites and thus blocks the reaction. The poisoning of certain active sites to inhibit an undesirable reaction is one of the strategies for developing selective catalysts for specific reactions.

The introduction of a second metal or a catalytically active oxide–metal interface can also change the selectivity. The dependence of the selectivity of benzene hydrogenation on the shape of the platinum nanoparticles of the same size shows the importance of the surface structure.[24]

8.2. Adsorbate-Induced Restructuring

Adsorbate-induced restructuring and adsorbate mobility (see Section 8.3) have been investigated by high-pressure scanning tunneling microscopy (HP-STM). STM has been a valuable technique for the study of surfaces in catalysis because it can operate over a wide range of pressures and temperatures, while providing spatial information of individual atoms or molecules in real space (Figure 16).[13,64–69] HP-STM measurements show that adsorption of a gas such as oxygen, hydrogen, or carbon monoxide changes the structure of the (110) surface of a platinum single crystal (Figure 17a).[70] During the chemisorption, there is an increased coverage of the different chemisorbed molecules under pressure which results in the chemical bond between the adsorbate and the substrate becoming stronger. The reversibility of adsorbate-induced restructuring was readily observed by a study of hydrogen adsorption on Cu(110).[69] Figure 17b shows STM images of a Cu(110) surface before and after exposure to H_2, and illustrates that under high pressure the adsorbate binding leads to (1×2) structures with missing rows. After evacuating the chamber, the original structure is once again obtained.

8.3. Adsorbate Mobility

The adsorbate mobility during catalytic turnover has been observed by high-pressure scanning tunneling microscopy.[65,71,72] No distinctive feature of the surface can be observed when scanning the surface at a rate of 100 Å per ms during the hydrogenation/dehydrogenation of cyclohexene or hydrogenation of ethylene. All the molecules on the surface—reactants, reaction intermediates, and products—are more mobile under these conditions than the scanning speed of the tunneling tip, and the products form (Figure 18). However, if the surface is poisoned using, for example, carbon monoxide, the catalytic reaction stops and there is an ordered structure formed on the surface. The poisoning of the catalyst also minimizes the mobility of the adsorbate. In many cases, adsorbate mobility is required for the catalytic process to occur, as the adsorbed reactants must find the active site and that requires mobility on the surfaces. The studies described in Sections 8.2 and 8.3 indicate that the catalytically active surface is dynamic: both the metal and the adsorbates restructure under the conditions of a catalytic reaction.

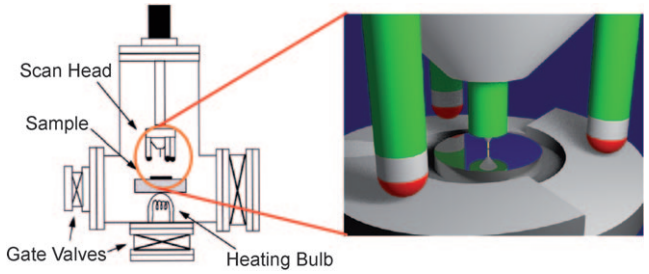

Figure 16. Schematic reprentation of a high-pressure scanning tunneling microscope.

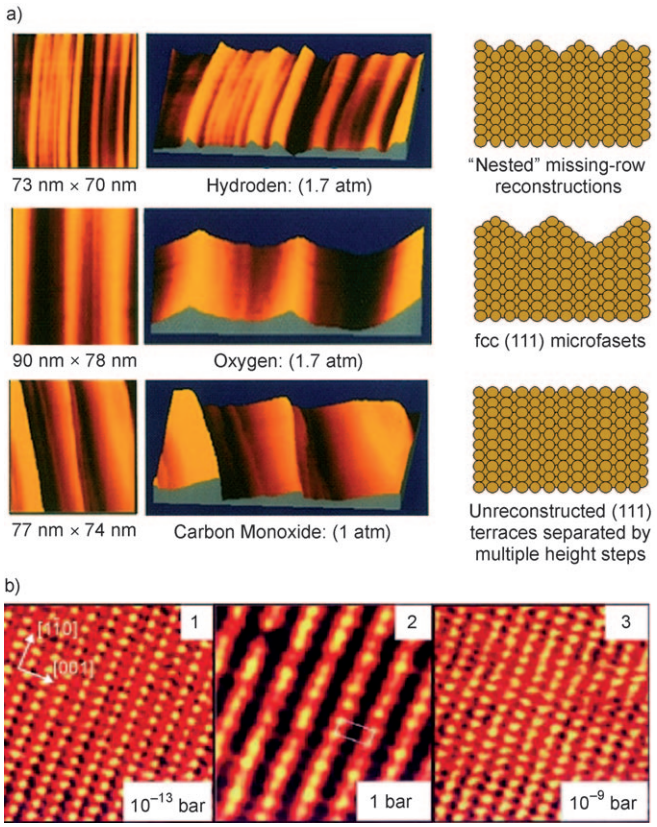

Figure 17. a) In situ STM images showing adsorbate-induced restructuring of a Pt(110) surface. b) STM topographical images showing Cu(110) before (1) and during H_2 exposure (2). At hydrogen pressures higher than 2 mbar the Cu(110) surface reconstructs into the (1×2) "missing row" structures. After evacuation, the adsorbate-induced restructuring is reversed and only a (1×1) surface structure (3) is revealed by STM.[69]

8.4. Reaction Intermediates

Sum frequency generation (SFG) vibrational spectroscopy is a surface-specific technique that was developed in

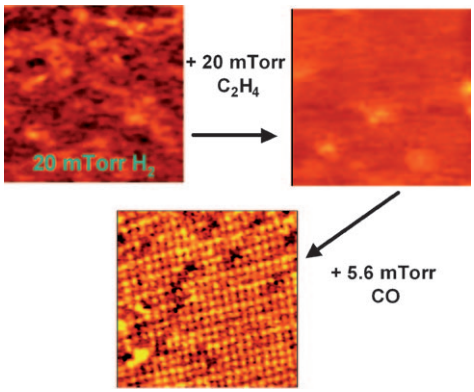

Figure 18. STM images of a Pt(111) surface after the sequential addition of 20 mTorr H_2, 20 mTorr C_2H_4, and 5.6 mTorr CO. Dimensions: 10 nm × 10 nm.

Berkeley and is based on the same principles as second harmonic generation.[14,64,73–78] Figure 19a shows a schematic representation of the experimental set up for analyzing a catalytic reaction by high-pressure SFG vibrational spectroscopy. In SFG, two laser beams in the IR and visible region are spatially and temporally overlapped. Scanning the frequency of the IR laser enables a sum frequency signal and, thus a vibrational spectra in the visible region, to be obtained (Figure 19b). Such a transition is symmetry forbidden for a centrosymmetric medium, such as the bulk phase of face-centered-cubic crystals or an isotropic high-pressure gas or a liquid. However, at the surface, the second order susceptibility ($\chi^{(2)}$) of non-zero is allowed (Figure 19c), and the surface yields a vibrational spectrum that is sensitive to the monolayer. Such a spectrum can also give us vibrational frequencies of adsorbed molecules across a pressure range of 10–12 orders of magnitude.[77,79]

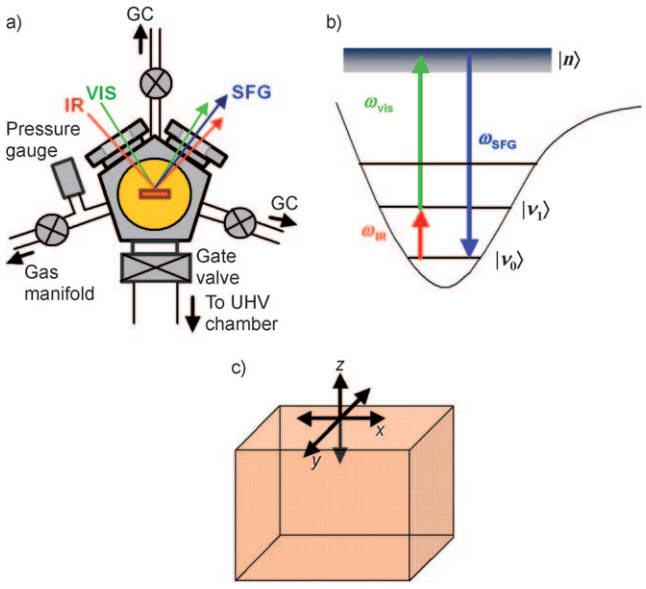

Figure 19. a) Schematic representation of a high-pressure SFG system, a vibrational spectroscopic tool for probing the adsorbed species during the catalytic reaction. b) The frequency ω_{vis} of the visible laser beam is held constant, and the frequency of the IR beam ω_{IR} is varied. When ω_{IR} coincides with a vibrational transition from $|0\rangle$ to $|1\rangle$ of an adsorbed molecule, the molecule is excited to a virtual state $|n\rangle$ and emits the sum frequency ω_{SFG}. c) As a consequence of the selection rule, SFG transitions from a centrosymmetric medium are forbidden; if $x=-x$, $y=-y$, and $z=-z$, then $\chi_{xyz}=\chi_{(-x)(-y)(-z)}=-\chi_{xyz}=0$. Typically, at an interface $z\neq -z$ and thus $\chi_{xyz}=\chi_{(-x)(-y)(-z)}=\chi_{xyz}$. Hence, $\chi^{(2)}\neq 0$, and a surface-specific signal is obtained.

The use of sum frequency generation vibrational spectroscopy enables reaction intermediates on the surface to be identified during catalytic turnover.[80–84] By measuring the turnover rate as well as the SFG signals, the kinetics of catalytic reactions can be related to reaction intermediates. For example, in the case of the hydrogenation of ethylene, some of the surface-bound species, such as ethylidyne and di-σ-bonded ethylene, are spectators and they do not participate in the hydrogenation of ethylene.[83,85] Weakly bound π-bonded ethylene, which will be converted into ethane, is present at only a concentration of 4% in the monolayer. Figure 20 shows the species that we see in the hydrogenation/dehydrogenation of cyclohexene.[86] During the hydrogenation/dehydrogenation cyclohexene, three reaction intermediates[84,87]—1,3-cyclohexadiene, 1,4-cyclohexadiene, and the π-allyl molecule—are observed, all of which participate at different concentrations, depending on the surface structure, in the formation of the products cyclohexane or benzene.

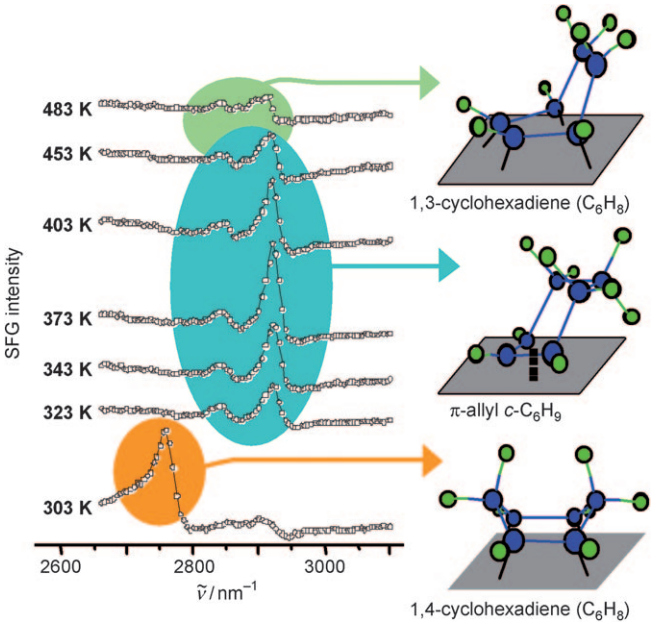

Figure 20. SFG spectra of the hydrogenation of cyclohexene to cyclohexane and the dehydrogenation of cyclohexene to benzene. These two reactions occur simultaneously in the presence of excess hydrogen (ca. 10 Torr) and 1.5 Torr of the hydrocarbon. The SFG vibration spectra reveal the presence of three different reaction intermediates on the surface: 1,4- and 1,3-cyclohexadiene as well as π-allyl c-C_6H_9.

High-pressure SFG can be used to study the reaction intermediates on the nanoparticle surfaces. Figure 21a shows a schematic representation of an SFG measurement on

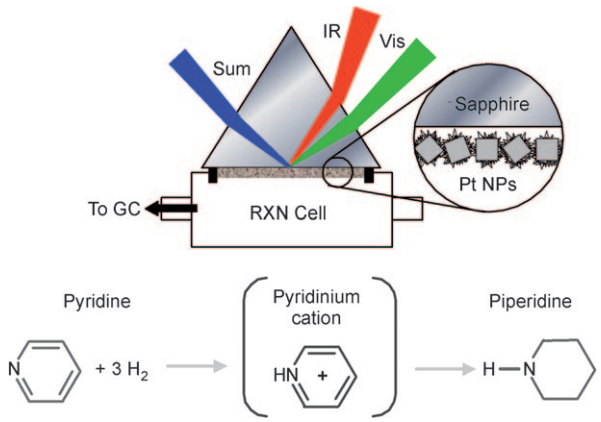

Figure 21. a) In situ monitoring of nanoparticles by high-pressure SFG spectroscopy. NP: nanoparticle. b) The pyridinium cation ($C_5H_5NH^+$) is present as a reaction intermediate in the hydrogenation of pyridine to piperidine.

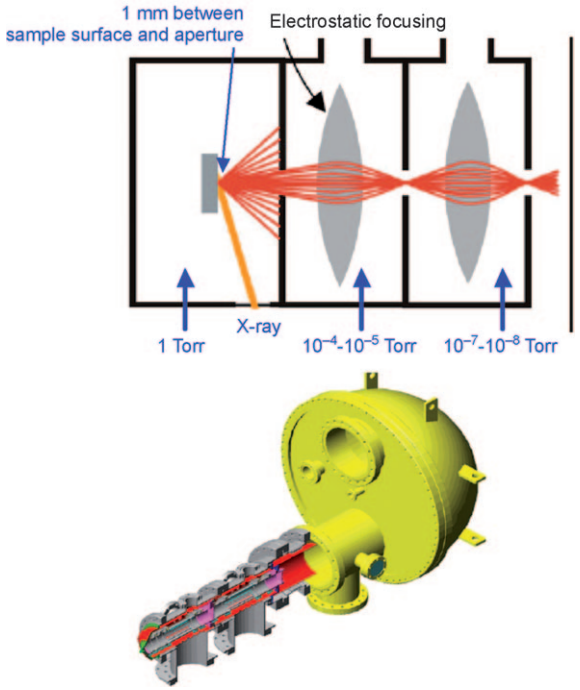

Figure 22. Schematic representation of ambient pressure X-ray photoelectron spectroscopy and differentially pumped electrostatic lens system and hemispherical analyzer.[15,94]

nanoparticles that are deposited on a prism, which allows for totally internal reflection to increase the detection sensitivity.[88] Our recent SFG studies on the hydrogenation of pyridine using this set up[89] revealed pyridinium ions ($C_5H_5NH^+$) as reaction intermediates on TTAB-covered platinum nanoparticles, and the formation of piperidine as the product of complete hydrogenation in the gas phase (Figure 21 b).

SFG-surface vibrational spectroscopy is able to detect reaction intermediates on the catalytically active surfaces under reaction conditions. Thus, direct observation of these intermediates gives another tool to obtain information on how reaction selectivity correlates with the molecular structure of the reaction intermediates.

8.5. Surface Composition

Surface composition is the key factor influencing the catalytic activity and selectivity of materials composed of two metals. The use of bimetallic nanoparticles allows the role of surface composition to be studied on the nanometer scale.[90–93]

For example, Rh_xPt_{1-x} nanoparticles with variable composition (x = 0–1) and constant size (9 ± 1) nm were synthesized by a one-pot polyol method, which utilizes the reduction kinetics of rhodium and platinum acetylacetonate in the nucleation and growth stage. The activity of these bimetallic nanoparticles in the oxidation of CO was studied. It was found that the turnover rate of a pure Rh nanoparticle is 20 times that of a Pt nanoparticle under the reaction conditions used (100 Torr O_2, 40 Torr CO at 180 °C), while Rh_xPt_{1-x} ($x = 0.2$–0.8) exhibits an intermediate activity.[28]

We studied the importance of the surface composition of platinum–rhodium nanoparticles by using ambient pressure X-ray photoelectron spectroscopy (AP-XPS). A schematic representation of AP-XPS is shown in Figure 22, which illustrates a differentially pumped electrostatic lens system that refocuses the scattered electrons into the object plane of a standard electron energy analyzer in the high-vacuum region.[15,94] (Details of the beamline and setup can be found in Ref. [95].) The kinetic energy of the detected electrons can be varied by tuning the photon energy of the X-ray source. This method permits the surface-specific XPS signal to be examined and the surface composition of the bimetallic nanoparticles to be determined.

Figure 23 a shows the XPS results of 8 nm sized $Rh_{0.5}Pt_{0.5}$ nanoparticles as a function of the kinetic energy of the X-rays, and shows the moderate surface segregation of rhodium. Our results also indicate that the surface composition changes as the reaction conditions are varied. Figure 23 b shows the change in the surface composition of the $Rh_{0.5}Pt_{0.5}$ nanoparticles, and the results suggest that Rh atoms are pulled to the surface during the oxidizing conditions of the reaction. This difference between the surface and the bulk composition will change the reaction rate and product distribution if both metals participate in the transformation.

Some bifunctional materials can be made by synthesizing an oxide or a sulfide coating around a metal nanoparticle. Two-component core–shell systems synthesized based on the Kirkendall effect[96] are also promising multicomponent nanocatalyst systems. TEM images of Pt nanoparticles and Pt@CoO core–shell nanostructures, often called nanoreactors, are shown in Figure 24.[97] These systems promise to be highly selective in reactions where active sites, both on the oxide and the metal, are important to produce the desired product, as long as the metal core is accessible to the reactant and product molecules through the porous oxide shell.

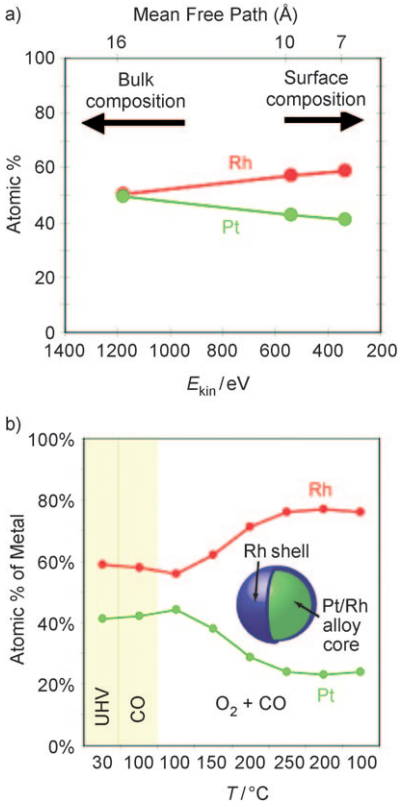

Figure 23. a) XPS results of 8 nm $Rh_{0.5}Pt_{0.5}$ nanoparticles as a function of the kinetic energy of the X-rays, which shows the moderate segregation of rhodium on the surface. b) High-pressure XPS results indicating greater segregation of rhodium on the surface under the reaction (oxidizing) conditions (kinetic energy of X-rays: 300 eV, and 60 mTorr of CO, and 150 mTorr of O_2). UHV = ultrahigh vacuum.

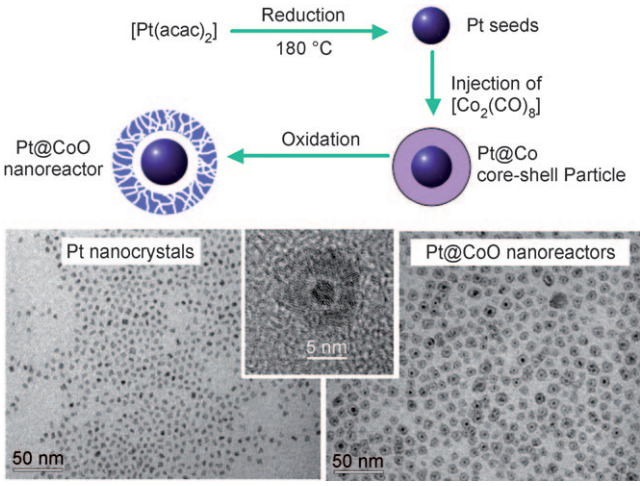

Figure 24. Synthesis of Pt@CoO core–shell nanostructures as well as TEM images of Pt and Pt@CoO core–shell nanoparticles.[97]

8.6. Charge Transport

Since the studies of Schwab in the 1950s, many others have indicated that the oxide–metal interface is a very active catalytic site.[31] The activity in the oxidation of methane ($CH_4 + 2O_2 \rightarrow CO_2 + 2H_2O$) was much higher with ZnO/Ag catalysts than with ZnO or Ag of the same weight (Figure 25 a).[32] The authors described the effect as follows:

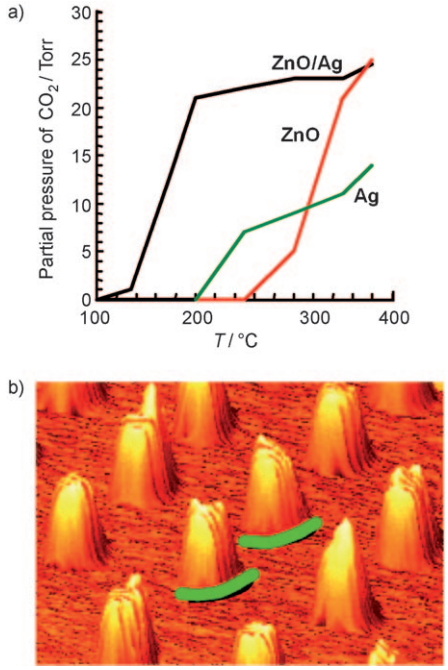

Figure 25. a) Plot of the CO_2 partial pressure in the oxidation of methane on ZnO/Ag, ZnO, and Ag catalysts of the same weight.[32] b) AFM image of platinum nanoparticles (50 nm) fabricated by lithography. The oxide–metal interface is highlighted in green.

"*The most striking factor is that the mixed catalyst gives an extremely high yield in water vapor and carbon dioxide*" and "*The catalytic promoter effect in a mixed catalyst is traced back to an electron exchange between support and catalyst*".[32]

After the study by Schwab and Koller, a whole family of catalysts—called "strong metal support interaction (SMSI) materials"—were developed, whose activity and selectivity is dependent on the oxide–metal interface.[33,98,99] These materials cover the Group VIII metals Fe, Ni, Rh, Pt, Pd, and Ir supported on certain oxides (TiO_x, TaO_x, CeO_x, and NbO_x). For example, Haller and Resasco found that the formation of methane from CO or CO_2 and H_2 is enhanced by three orders of magnitude on a SMSI material compared to non-SMSI supports.[33,100] Figure 25 b shows the AFM image of a platinum nanoparticle, with the chemically active oxide–metal interface highlighted, fabricated by using a lithography technique.[35,36]

The interaction between the oxide support and the metal catalyst has been attributed to either geometric or electronic effects.[8,33,101] The geometrical effect assumes that the active surface area of the noble metal is changed during the reduction process. The electronic effect involves charge transfer between the metal and the oxide support. This effect was also investigated by Boffa et al. using various oxides deposited on rhodium for CO_2 hydrogenation.[102] They observed a remarkable 14-fold increase in turnover rates, especially in the presence of TiO_x, NbO_x, and TaO_x. The

activity was at a maximum when the oxide–metal interface area was at a maximum, which occurred when the oxide coverage corresponded to one-half of a monolayer. Recently, the generation of "hot" electrons during exothermic reaction conditions or in the presence of photons has revealed probable reasons for the change in the chemical activity at the oxide–metal interface.[2,38,41,59,103–106]

During exothermic chemical processes, energetic charge carriers can be generated through the non-adiabatic electronic dissipation of chemical energy. Experimental evidence indicating the presence of energetic ("hot") electrons has been reported. Pump-probe experiments carried out on femtosecond time scales have detected the presence of electrons with kinetic energies of 1–3 eV that have elastic mean-free paths of approximately 10 nm in metals. Several experiments suggest that the electronic excitation causes adsorption and desorption of atoms and molecules or the dissociation of molecules. Nienhaus et al. detected electrons with a kinetic energy greater than 0.5 eV when hydrogen or oxygen atoms adsorbed on a silver thin film Schottky diode were injected. The "hot" electrons travel in excess of the electron mean-free path in silver (ca. 20 nm) and surmount the Schottky barrier of about 0.5 eV formed at the junction of the silver and the underlying semiconductor.[40,41,107]

We fabricated a metal–semiconductor Schottky diode to detect this flow of "hot" electrons.[38,39,106,108] If the metal particle[59] or film[109] is of the diameter or thickness of the mean free path of electrons (ca. 10 nm), "hot" electrons can be collected as they are transported across the metal without collision (Figure 26a). For an n-type Schottky diode, "hot" electrons are detected as a chemical current if their excess energy $E_{ex} = |E - E_F|$ is larger than the effective Schottky barrier, which is the difference between the conduction band minimum and the Fermi energy E_F at the interface. Once "hot" electrons arrive at the oxide, they dissipate energy and, thus, cannot go back to the metal. Therefore, the Schottky energy barrier leads to an irreversible, one-way charge transfer of "hot" electrons from the metal to the semiconductor. After the "hot" electrons have moved from the metal to the semiconductor, they are replaced by low-energy electrons supplied by the external leads connected to the platinum and semiconductor. This results in the generation of a continuous flow of "hot" electrons by the catalytic reaction.

Our nanodiode catalyst consists of a 5 nm platinum thin film on a semiconducting film (titanium dioxide or gallium nitride) with gold pads for Ohmic contact to the platinum and semiconductor (Figure 26b). We found that the flow of "hot" electrons is correlated with the turnover rate of CO oxidation measured with the Pt/GaN diode (Figure 26c).[109,110] This experiment clearly verifies that the chemical energy in the catalytic reaction is converted into the kinetic energy of the flowing "hot" electrons.

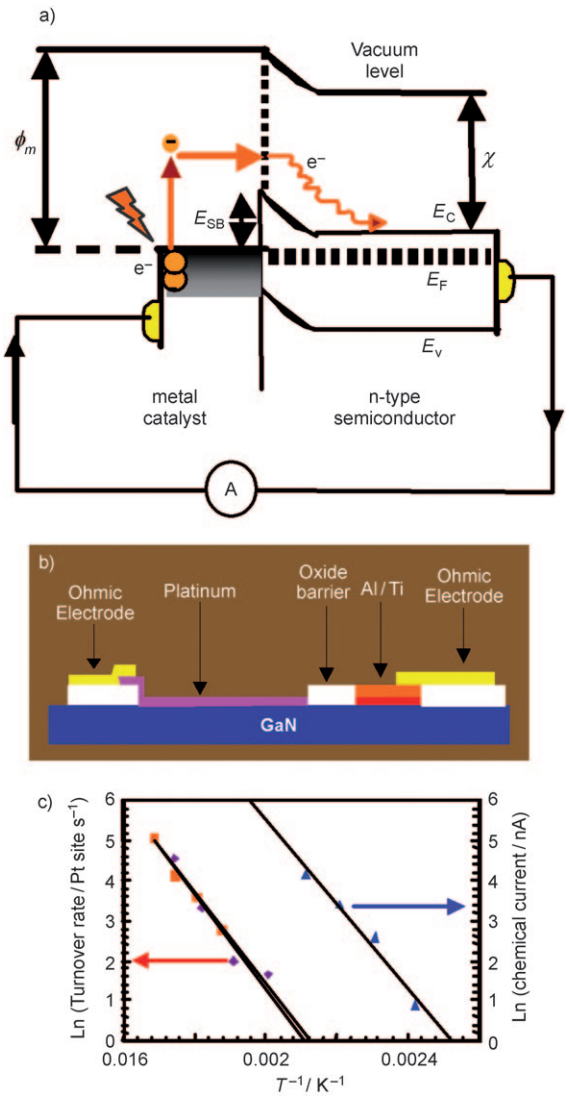

Figure 26. a) Detection of moving charge carriers in a Schottky diode constructed from a metal catalyst and a semiconductor. b) Schematic representation of the Pt/GaN nanodiode. c) Logarithmic plot of chemical current and turnover rate as a function of temperature during the oxidation of carbon monoxide. A correlation between the flow of "hot" electrons and catalytic reactions is evident.

8.7. Oxidation States

Platinum and rhodium nanoparticles around 1 nm or smaller can be synthesized using dendrimers as a support. The smaller the nanoparticles are, the greater their oxidation.[22] The size dependence of the oxidation state leads to a different chemical behavior for small clusters of atoms, which may approach the behavior of homogeneous catalysts.[111–114] Figure 27a,b show XPS results of Pt_{20} (0.8 nm in size) and Pt_{40} clusters (1.5 nm in size), respectively. It is evident that the oxidation states of these small, nonmetallic nanoparticles depend on the particle size.[55] In the case of Pt_{20}, the Pt 4f signal gives a Pt^{x+}/Pt^0 ratio of 13:1. By controlling the oxidation state by the size of the clusters, they could be used, for example, in hydroformylation and carbonylation reactions, which at present are performed with homogeneous catalysts. Future studies will show how catalysts can be prepared by depositing size-controlled metal clusters in dendrimers or other supports, thereby making it easier to separate the catalysts (which are heterogeneous) from the reactants and products.

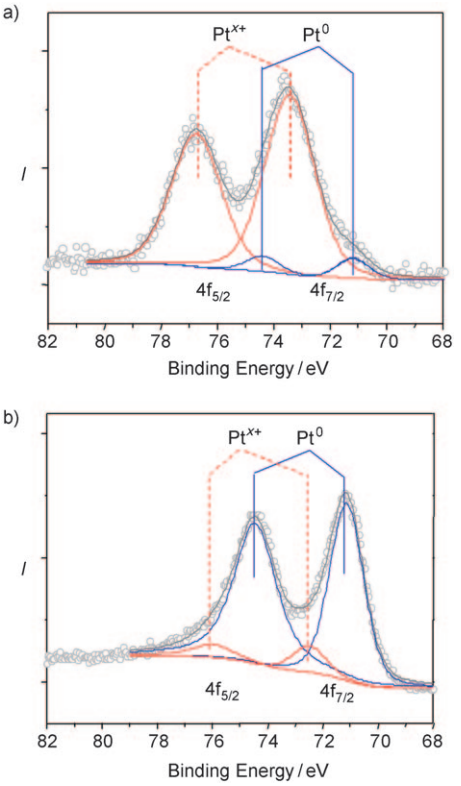

Figure 27. XPS results of a) Pt_{20} nanoparticles (0.8 nm) and b) Pt_{40} nanoparticles (1.5 nm). The Pt^{x+}/Pt^0 ratio of the Pt_{20} and Pt_{40} nanoparticles are 13:1 and 0.16:1, respectively. In Pt_{20}, the higher oxidation state of Pt is thus dominant.

9. Future Perspective

The field of nanocatalysis is concerned with monodispersed metal nanoparticles of controlled size and shape, and involves synthesis, characterization, and reaction studies in both two and three dimensions. This integrated approach has given the field of catalysis a new impetus at a time when energy efficiency and chemical selectivity (green chemistry) are major societal goals. Scientists today need to carry out synthesis, characterization, and reaction studies themselves, three aspects of catalytic studies that were partitioned in the past. In this way, the same person can use the knowledge gained from reaction studies on the synthesis and characterization of what has been found to successfully produce selective catalysts by controlled methods. This approach not only accelerates research progress but permits the rapid transfer of results from model systems to catalyst design for the chemical technologies. New generations of industrial catalysts are already being produced by using results from model systems. Examples include the Cu/ZnO catalyst for the synthesis of methanol and a new hydrodesulfurization catalyst from the Haldor Topsoe company[115–117] as well as the new generation of catalytic converters for automobiles that have better selectivity, turnover rates, and stability against deactivation. It is likely that industry will convert from the catalyst fabrication pioneered by Mittasch in the 1930s[118] and the wet impregnation method[119] pioneered by Universal Oil Products in the 1940s to high technology fabrication methods suggested by studies on model nanocatalysts. Such model systems are also necessary for other reaction conditions, such as at high reaction temperatures (combustion and cracking) and at solid–liquid interfaces.

The nanomaterial technology that allows catalysts to be made in a controlled way with sizes of 1–10 nm and with a defined shape brings the dream closer of uniting the three fields of catalysis: enzyme, homogeneous, and heterogeneous. Since enzymes mostly operate at temperatures around 300 K and in solution (which is most often aqueous, although organic solvents can frequently be used), it would be important to carry out catalytic reaction studies with heterogeneous and homogeneous catalysts under these conditions. In this way, it would perhaps be possible to correlate the molecular factors of the three catalyst types and develop hybrid systems that take advantage of, for example, enzyme selectivity in a heterogeneous medium. The future is indeed bright for catalysis science viewed from the perspective of nanocatalysis.

This paper is based on the plenary lecture presented at the International Symposium on Creation and Control of Advanced Selective Catalysis, Kyoto, Japan. The work presented in this Review was supported by the Director, Office of Science, Office of Basic Energy Sciences, Division of Materials Sciences and Engineering of the U.S. Department of Energy under Contract No. DE-AC02-05CH11231.

Received: July 2, 2008

[1] G. A. Somorjai, *Introduction to Surface Chemistry and Catalysis*, Wiley, New York, **1994**.
[2] G. A. Somorjai, K. M. Bratlie, M. O. Montano, J. Y. Park, *J. Phys. Chem. B* **2006**, *110*, 20014.
[3] G. A. Somorjai, J. Y. Park, *Catal. Lett.* **2007**, *115*, 87.
[4] J. H. Clark, *Green Chem.* **1999**, *1*, 1.
[5] A. Corma, *Chem. Rev.* **1997**, *97*, 2373.
[6] C. T. Kresge, M. E. Leonowicz, W. J. Roth, J. C. Vartuli, J. S. Beck, *Nature* **1992**, *359*, 710.
[7] D. Zhao, P. Yang, N. Melosh, J. Feng, B. F. Chmelka, G. D. Stucky, *Adv. Mater.* **1998**, *10*, 1380.
[8] K. Hayek, M. Fuchs, B. Klotzer, W. Reichl, G. Rupprechter, *Top. Catal.* **2000**, *13*, 55.
[9] R. Narayanan, M. A. El-Sayed, *Nano Lett.* **2004**, *4*, 1343.
[10] Y. Borodko, S. M. Humphrey, T. D. Tilley, H. Frei, G. A. Somorjai, *J. Phys. Chem. C* **2007**, *111*, 6288.
[11] H. Song, F. Kim, S. Connor, G. A. Somorjai, P. D. Yang, *J. Phys. Chem. B* **2005**, *109*, 188.
[12] G. A. Somorjai, J. Y. Park, *J. Chem. Phys.* **2008**, *128*, 182504.
[13] K. B. Rider, K. S. Hwang, M. Salmeron, G. A. Somorjai, *J. Am. Chem. Soc.* **2002**, *124*, 5588.
[14] Y. R. Shen, *Nature* **1989**, *337*, 519.
[15] M. Salmeron, R. Schlogl, *Surf. Sci. Rep.* **2008**, *63*, 169.
[16] G. A. Somorjai, J. Y. Park, *Phys. Today* **2007**, *60*, 48.
[17] F. Zaera, *J. Phys. Chem. B* **2002**, *106*, 4043.
[18] G. A. Somorjai, Y. G. Borodko, *Catal. Lett.* **2001**, *76*, 1.
[19] P. B. Weisz, *Pure Appl. Chem.* **1980**, *52*, 2091.
[20] G. A. Somorjai, M. C. Yang, *Top. Catal.* **2003**, *24*, 61.
[21] G. A. Somorjai, R. M. Rioux, *Catal. Today* **2005**, *100*, 201.
[22] I. Balint, A. Miyazaki, K. Aika, *J. Catal.* **2003**, *220*, 74.

[23] C. Mohr, H. Hofmeister, J. Radnik, P. Claus, *J. Am. Chem. Soc.* **2003**, *125*, 1905.
[24] K. M. Bratlie, H. Lee, K. Komvopoulos, P. Yang, G. A. Somorjai, *Nano Lett.* **2007**, *7*, 3097.
[25] G. Ertl, H. J. Freund, *Phys. Today* **1999**, *52*, 32.
[26] W. S. Caughey, G. A. Smythe, D. H. Okeeffe, J. E. Maskasky, M. L. Smith, *J. Biol. Chem.* **1975**, *250*, 7602.
[27] N. Tian, Z. Y. Zhou, S. G. Sun, Y. Ding, Z. L. Wang, *Science* **2007**, *316*, 732.
[28] J. Y. Park, Y. Zhang, M. Grass, T. Zhang, G. A. Somorjai, *Nano Lett.* **2008**, *8*, 673.
[29] H. J. Freund, H. Kuhlenbeck, J. Libuda, G. Rupprechter, M. Baumer, H. Hamann, *Top. Catal.* **2001**, *15*, 201.
[30] G. A. Somorjai, R. L. York, D. Butcher, J. Y. Park, *Phys. Chem. Chem. Phys.* **2007**, *9*, 3500.
[31] G. M. Schwab, *Angew. Chem.* **1967**, *79*, 325; *Angew. Chem. Int. Ed. Engl.* **1967**, *6*, 375.
[32] G. M. Schwab, K. Koller, *J. Am. Chem. Soc.* **1968**, *90*, 3078.
[33] G. L. Haller, D. E. Resasco, *Adv. Catal.* **1989**, *36*, 173.
[34] G. A. Somorjai, F. Tao, J. Y. Park, *Top. Catal.* **2008**, *47*, 1.
[35] J. Grunes, J. Zhu, E. A. Anderson, G. A. Somorjai, *J. Phys. Chem. B* **2002**, *106*, 11463.
[36] J. Grunes, J. Zhu, M. C. Yang, G. A. Somorjai, *Catal. Lett.* **2003**, *86*, 157.
[37] X. M. Yan, A. M. Contreras, M. M. Koebel, J. A. Liddle, G. A. Somorjai, *Nano Lett.* **2005**, *5*, 1129.
[38] X. Z. Ji, G. A. Somorjai, *J. Phys. Chem. B* **2005**, *109*, 22530.
[39] X. Z. Ji, A. Zuppero, J. M. Gidwani, G. A. Somorjai, *J. Am. Chem. Soc.* **2005**, *127*, 5792.
[40] H. Nienhaus, H. S. Bergh, B. Gergen, A. Majumdar, W. H. Weinberg, E. W. McFarland, *Phys. Rev. Lett.* **1999**, *82*, 446.
[41] H. Nienhaus, B. Gergen, W. H. Weinberg, E. W. McFarland, *Surf. Sci.* **2002**, *514*, 172.
[42] Y. Zhang, M. E. Grass, S. E. Habas, F. Tao, T. Zhang, P. Yang, G. A. Somorjai, *J. Phys. Chem. C* **2007**, *111*, 12243.
[43] R. M. Rioux, H. Song, M. Grass, S. Habas, K. Niesz, J. D. Hoefelmeyer, P. Yang, G. A. Somorjai, *Top. Catal.* **2006**, *39*, 167.
[44] H. Lee, S. E. Habas, S. Kweskin, D. Butcher, G. A. Somorjai, P. D. Yang, *Angew. Chem.* **2006**, *118*, 7988; *Angew. Chem. Int. Ed.* **2006**, *45*, 7824.
[45] Y. W. Zhang, M. E. Grass, J. N. Kuhn, F. Tao, S. E. Habas, W. Y. Huang, P. D. Yang, G. A. Somorjai, *J. Am. Chem. Soc.* **2008**, *130*, 5868.
[46] S. M. Humphrey, M. E. Grass, S. E. Habas, K. Niesz, G. A. Somorjai, T. D. Tilley, *Nano Lett.* **2007**, *7*, 785.
[47] M. E. Grass, Y. Yue, S. E. Habas, R. M. Rioux, C. I. Teall, P. Yang, G. A. Somorjai, *J. Phys. Chem. C* **2008**, *112*, 4797.
[48] H. Song, R. M. Rioux, J. D. Hoefelmeyer, R. Komor, K. Niesz, M. Grass, P. D. Yang, G. A. Somorjai, *J. Am. Chem. Soc.* **2006**, *128*, 3027.
[49] G. A. Somorjai, J. Y. Park, *Top. Catal.* **2008**, *49*, 126.
[50] R. M. Crooks, M. Q. Zhao, L. Sun, V. Chechik, L. K. Yeung, *Acc. Chem. Res.* **2001**, *34*, 181.
[51] Y. H. Niu, L. K. Yeung, R. M. Crooks, *J. Am. Chem. Soc.* **2001**, *123*, 6840.
[52] Y. Li, M. A. El-Sayed, *J. Phys. Chem. B* **2001**, *105*, 8938.
[53] K. R. Gopidas, J. K. Whitesell, M. A. Fox, *Nano Lett.* **2003**, *3*, 1757.
[54] R. W. J. Scott, O. M. Wilson, R. M. Crooks, *J. Phys. Chem. B* **2005**, *109*, 692.
[55] W. Huang, J. N. Kuhn, C. K. Tsung, Y. Zhang, S. E. Habas, P. Yang, G. A. Somorjai, *Nano Lett.* **2008**, *8*, 2027.
[56] D. Y. Zhao, J. L. Feng, Q. S. Huo, N. Melosh, G. H. Fredrickson, B. F. Chmelka, G. D. Stucky, *Science* **1998**, *279*, 548.
[57] P. Schmidt-Winkel, W. W. Lukens, D. Y. Zhao, P. D. Yang, B. F. Chmelka, G. D. Stucky, *J. Am. Chem. Soc.* **1999**, *121*, 254.
[58] K. M. Bratlie, C. J. Kliewer, G. A. Somorjai, *J. Phys. Chem. B* **2006**, *110*, 17925.
[59] J. Y. Park, H. Lee, J. R. Renzas, Y. Zhang, G. A. Somorjai, *Nano Lett.* **2008**, *8*, 2388.
[60] J. R. Vig, *J. Vac. Sci. Technol. A* **1985**, *3*, 1027.
[61] C. Aliaga, J. Y. Park, Y. Yamada, G. A. Somorjai, unpublished results.
[62] S. M. Davis, F. Zaera, G. A. Somorjai, *J. Am. Chem. Soc.* **1982**, *104*, 7453.
[63] G. A. Somorjai, *React. Kinet. Catal. Lett.* **1987**, *35*, 37.
[64] G. A. Somorjai, X. C. Su, K. R. McCrea, K. B. Rider, *Top. Catal.* **1999**, *8*, 23.
[65] M. Montano, M. Salmeron, G. A. Somorjai, *Surf. Sci.* **2006**, *600*, 1809.
[66] M. Montano, D. C. Tang, G. A. Somorjai, *Catal. Lett.* **2006**, *107*, 131.
[67] S. R. Longwitz, J. Schnadt, E. K. Vestergaard, R. T. Vang, E. Laegsgaard, I. Stensgaard, H. Brune, F. Besenbacher, *J. Phys. Chem. B* **2004**, *108*, 14497.
[68] B. L. M. Hendriksen, J. W. M. Frenken, *Phys. Rev. Lett.* **2002**, *89*, 046101.
[69] L. Osterlund, P. B. Rasmussen, P. Thostrup, E. Laegsgaard, I. Stensgaard, F. Besenbacher, *Phys. Rev. Lett.* **2001**, *86*, 460.
[70] B. J. McIntyre, M. Salmeron, G. A. Somorjai, *J. Vac. Sci. Technol. A* **1993**, *11*, 1964.
[71] M. Montano, K. Bratlie, M. Salmeron, G. A. Somorjai, *J. Am. Chem. Soc.* **2006**, *128*, 13229.
[72] D. C. Tang, K. S. Hwang, M. Salmeron, G. A. Somorjai, *J. Phys. Chem. B* **2004**, *108*, 13300.
[73] G. Rupprechter, *MRS Bull.* **2007**, *32*, 1031.
[74] Y. R. Shen, *Annu. Rev. Phys. Chem.* **1989**, *40*, 327.
[75] K. Y. Kung, P. Chen, F. Wei, Y. R. Shen, G. A. Somorjai, *Surf. Sci.* **2000**, *463*, L627.
[76] O. Mermut, D. C. Phillips, R. L. York, K. R. McCrea, R. S. Ward, G. A. Somorjai, *J. Am. Chem. Soc.* **2006**, *128*, 3598.
[77] X. C. Su, P. S. Cremer, Y. R. Shen, G. A. Somorjai, *J. Am. Chem. Soc.* **1997**, *119*, 3994.
[78] S. Westerberg, C. Wang, G. A. Somorjai, *Surf. Sci.* **2005**, *582*, 137.
[79] X. C. Su, J. Jensen, M. X. Yang, M. B. Salmeron, Y. R. Shen, G. A. Somorjai, *Faraday Discuss.* **1996**, *105*, 263.
[80] K. M. Bratlie, L. D. Flores, G. A. Somorjai, *J. Phys. Chem. B* **2006**, *110*, 10051.
[81] Z. Chen, D. H. Gracias, G. A. Somorjai, *Appl. Phys. B* **1999**, *68*, 549.
[82] P. Cremer, C. Stanners, J. W. Niemantsverdriet, Y. R. Shen, G. Somorjai, *Surf. Sci.* **1995**, *328*, 111.
[83] P. S. Cremer, X. C. Su, Y. R. Shen, G. A. Somorjai, *Catal. Lett.* **1996**, *40*, 143.
[84] M. Yang, G. A. Somorjai, *J. Am. Chem. Soc.* **2003**, *125*, 11131.
[85] P. S. Cremer, X. C. Su, Y. R. Shen, G. A. Somorjai, *J. Am. Chem. Soc.* **1996**, *118*, 2942.
[86] K. M. Bratlie, L. D. Flores, G. A. Somorjai, *Surf. Sci.* **2005**, *599*, 93.
[87] M. C. Yang, R. M. Rioux, G. A. Somorjai, *J. Catal.* **2006**, *237*, 255.
[88] S. J. Kweskin, R. M. Rioux, S. E. Habas, K. Komvopoulos, P. Yang, G. A. Somorjai, *J. Phys. Chem. B* **2006**, *110*, 15920.
[89] K. M. Bratlie, K. Komvopoulos, G. A. Somorjai, *J. Phys. Chem. C* **2008**, *112*, 11865.
[90] L. E. Aleandri, H. Bonnemann, D. J. Jones, J. Richter, J. Roziere, *J. Mater. Chem.* **1995**, *5*, 749.
[91] J. A. Rodriguez, D. W. Goodman, *Science* **1992**, *257*, 897.
[92] J. Rothe, G. Kohl, J. Hormes, H. Bonnemann, W. Brijoux, K. Siepen, *J. Phys. IV* **1997**, *7*, C2–959.
[93] N. Toshima, T. Yonezawa, *New J. Chem.* **1998**, *22*, 1179.

[94] H. Bluhm, M. Havecker, A. Knop-Gericke, M. Kiskinova, R. Schlogl, M. Salmeron, *MRS Bull.* **2007**, *32*, 1022.
[95] D. F. Ogletree, H. Bluhm, G. Lebedev, C. S. Fadley, Z. Hussain, M. Salmeron, *Rev. Sci. Instrum.* **2002**, *73*, 3872.
[96] A. D. Smigelskas, E. O. Kirkendall, *Trans. Am. Inst. Min. Metall. Eng.* **1947**, *171*, 130.
[97] Y. D. Yin, R. M. Rioux, C. K. Erdonmez, S. Hughes, G. A. Somorjai, A. P. Alivisatos, *Science* **2004**, *304*, 711.
[98] S. J. Tauster, S. C. Fung, R. L. Garten, *J. Am. Chem. Soc.* **1978**, *100*, 170.
[99] K. Foger in *Catalysis, Science and Technology*, *Vol. 6* (Eds.: J. R. Anderson, M. Boudart), Springer, Berlin, **1984**, chap. 4.
[100] J. P. Hindermann, G. J. Hutchings, A. Kiennemann, *Catal. Rev. Sci. Eng.* **1993**, *35*, 1.
[101] R. Burch in *Hydrogen Effects in Catalysis* (Eds.: Z. Páal, P. G. Menon), Dekker, New York, **1988**, p. 347.
[102] A. Boffa, C. Lin, A. T. Bell, G. A. Somorjai, *J. Catal.* **1994**, *149*, 149.
[103] Y. H. Huang, C. T. Rettner, D. J. Auerbach, A. M. Wodtke, *Science* **2000**, *290*, 111.
[104] J. W. Gadzuk, *J. Phys. Chem. B* **2002**, *106*, 8265.
[105] H. Nienhaus, S. J. Weyers, B. Gergen, E. W. McFarland, *Sens. Actuators B* **2002**, *87*, 421.
[106] J. Y. Park, G. A. Somorjai, *J. Vac. Sci. Technol. B* **2006**, *24*, 1967.
[107] H. Nienhaus, *Surf. Sci. Rep.* **2002**, *45*, 1.
[108] J. Y. Park, J. R. Renzas, A. M. Contreras, G. A. Somorjai, *Top. Catal.* **2007**, *46*, 217.
[109] J. Y. Park, J. R. Renzas, B. B. Hsu, G. A. Somorjai, *J. Phys. Chem. C* **2007**, *111*, 15331.
[110] J. Y. Park, G. A. Somorjai, *ChemPhysChem* **2006**, *7*, 1409.
[111] M. D. Ackermann, T. M. Pedersen, B. L. M. Hendriksen, O. Robach, S. C. Bobaru, I. Popa, C. Quiros, H. Kim, B. Hammer, S. Ferrer, J. W. M. Frenken, *Phys. Rev. Lett.* **2005**, *95*, 255505.
[112] M. S. Chen, Y. Cal, Z. Yan, K. K. Gath, S. Axnanda, D. W. Goodman, *Surf. Sci.* **2007**, *601*, 5326.
[113] H. Gabasch, A. Knop-Gericke, R. Schlogl, M. Borasio, C. Weilach, G. Rupprechter, S. Penner, B. Jenewein, K. Hayek, B. Klotzer, *Phys. Chem. Chem. Phys.* **2007**, *9*, 533.
[114] N. Lopez, T. V. W. Janssens, B. S. Clausen, Y. Xu, M. Mavrikakis, T. Bligaard, J. K. Norskov, *J. Catal.* **2004**, *223*, 232.
[115] J. D. Grunwaldt, A. M. Molenbroek, N. Y. Topsoe, H. Topsoe, B. S. Clausen, *J. Catal.* **2000**, *194*, 452.
[116] N. Y. Topsoe, H. Topsoe, *Top. Catal.* **1999**, *8*, 267.
[117] K. G. Knudsen, B. H. Cooper, H. Topsoe, *Appl. Catal. A* **1999**, *189*, 205.
[118] A. Mittasch, E. Keunecke, *Z. Elektrochem. Angew. Phys. Chem.* **1932**, *38*, 666.
[119] J. Yang, V. Tschamber, D. Habermacher, F. Garin, P. Gilot, *Applied Catalysis B: Environmental* **2008**, *83*, 229.

